SN Computer Science (2024) 5:224
https://doi.org/10.1007/s42979-023-02502-9

ORIGINAL RESEARCH

50-Channel Ionoacoustic Sensor for 60 MeV Proton Beam Characterization in Hadron Therapy Applications

Elia Arturo Vallicelli[1] · Mattia Tambaro[1] · Mattia Oliver Cosmi[1] · Andrea Baschirotto[1] · Marcello De Matteis[1]

Received: 25 October 2021 / Accepted: 25 August 2022 / Published online: 20 January 2024

Abstract

This paper presents the design of a piezoelectric multichannel sensor optimized for sensing weak ionoacoustic signals generated at the Bragg peak (BP) of pulsed proton beams, with interesting possible applications in real-time monitoring of oncological hadron therapy treatments. To overcome current single-channel detector limitations and acquire the weak acoustic signals of clinical scenarios (60–200 MeV proton energy and few mGy dose deposition), the hereby presented detector overcomes the state-of-the-art approach (based on time-domain correlation i.e., averaging different beam pulses) by using spatial correlation (i.e., averaging signals from different detector channels) to increase the SNR without increasing the delivered dose. The detector design is tailored around the experimental environment characteristics (signal amplitude, signal frequency, relative BP-detector position) of a clinical proton beam (60 MeV, 2 mGy/pulse dose deposition). The detector design was characterized by a complete cross-domain simulation of the physical (proton beam), acoustic (wave propagation) and electrical (sensor and electronics frequency response and noise) environments. It achieves a clear 10 dB single-pulse SNR (2 mGy total dose) and allows to locate the BP with 125 µm precision (<3% w.r.t. the particle range). Finally, the detector was experimentally validated by a piezoelectric acoustic testbench and has shown the capability to localize an acoustic source in 2D with sub-millimeter accuracy by using a multilateration-based BP detection algorithm.

Keywords Nuclear imaging · Particle accelerator · Particle beam measurements · Acoustic waves · Analog circuits and digital circuits

Introduction

The ionacoustic effect consists in the generation of an acoustic signal in the region of the Bragg peak of pulsed particle beams. Charged particles beams (e.g. protons) deposit their energy in an energy absorber (e.g., water tank) following the Bragg curve (Fig. 1), characterized by a maximum deposition at the end of the particle range [1]. The ionoacoustic signal generated by the rapid deposition of energy is propagated in the absorber in the form of an acoustic wave that can be acquired by a dedicated ionoacoustic detector [2, 3]. By measuring the acoustic wave time of flight, it is possible to localize the BP with high precision [4, 5]. For this reason, ionacoustic detectors are studied for their potential applications in medical physics [6]. In particular, the ionoacoustic effect is very promising as a monitoring tool in oncological hadron therapy treatments, where it promises greater precision (sub-millimeter vs. several millimeters) and greater detector simplicity (piezoelectric vs. photomultipliers) compared to currently used nuclear imaging techniques (positron emission tomography, prompt gamma ray imaging).

However, the state of the art of ionacoustic experiments use general-purpose detectors with limited performance in terms of noise power. This lowers the signal-to-noise ratio (SNR) and increases the error associated with the measurements, preventing clinical applications of current ionoacoustic detectors [7, 8]. In fact, the ionoacoustic signals produced during hadron therapy treatments have amplitudes 10–20 dB lower than the noise background of the current ionoacoustic detectors. To improve the SNR, post-processing algorithms (time-domain averaging of up to 1000 different beam pulses)

This article is part of the topical collection "Biomedical Engineering Systems and Technologies" guest edited by Hugo Gamboa and Ana Fred.

✉ Elia Arturo Vallicelli
eliaarturo.vallicelli@unimib.it

[1] Bicocca and the Italian Institute for Nuclear Physics (INFN), University of Milano, Milan, Italy

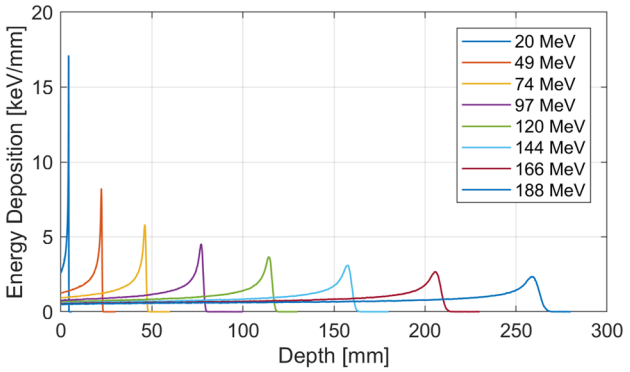

Fig. 1 Bragg curve for protons of different pre-clinical (<60 MeV) and clinical (60–200 MeV) energies

are applied [9, 10]. However, since each beam pulse delivers an additional dose, the extra dose required by current detectors greatly exceeds clinical limits, effectively preventing the application of this technique during treatments [11, 12].

To overcome this limitation, this paper presents the development and experimental characterization of a low noise multichannel acoustic sensor that significantly improves the SNR by leveraging on two fundamental points:

The frequency response of the acoustic sensor copies the acoustic signal bandwidth, maximizing the sensitivity of the detector and rejecting out-of-band noise and interference.

Combining the signals acquired by a multichannel sensor allows to perform spatial domain averaging, rejecting in-band noise and increasing the SNR without extra dose.

This paper describes the design and characterization of a detector optimized for 60 MeV clinical proton beams and is organized as follows.

60 Mev Proton Beam Experimental Scenario

The typical experimental setup for ionoacoustic experiments consists of a water tank inside which the proton beam deposits its energy and generates the ionoacoustic signal. One or more acoustic sensors detect the signal which is then processed in the analog and digital domain by a dedicated front-end. Figure 2 shows a k-Wave simulation of this process. The most intense ionacoustic signal is generated in the Bragg peak and its characteristics in terms of frequency and amplitude are dependent on the FWHM dimension of the BP and on the deposited dose, respectively. These characteristics of the BP depend mainly on the energy of the beam, which reaches higher ranges as the energy increases, as shown in Fig. 3. As the range increases, the physical size of the

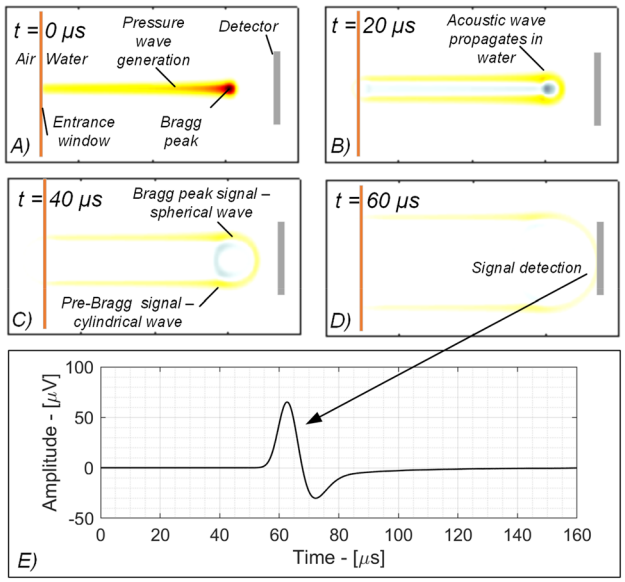

Fig. 2 k-Wave simulation of the ionoacoustic effect. **A** Pressure increase at $t=0$. **B** Acoustic signal propagation. **C** Highlight of Pre-Bragg and BP acoustic signals. **D** Acoustic wave is sensed by the detector. E) Acoustic signal time track

BP also increases, whose FWHM increases (BP_{FWHM}) [13, 14]. The wavelength of the ionoacoustic signal is directly proportional to the BP_{FWHM}. While at sub-clinical energies the frequencies (i.e., inverse of the period) of the acoustic signals are in the order of few MHz, in the clinical range (60–200 MeV) the signal drops below 500 kHz, as shown in Fig. 4. The amplitude of the acoustic signal is directly proportional to the dose deposited in the Bragg peak in each pulse when the stress and thermal confinement conditions are respected. Most clinical treatments deposit a total dose of a few Gy, divided into fractions of a few tens of mGy per beam pulse. This results in a signal of a few hundred mPa at BP that is then attenuated by 20–30 dB by spherical

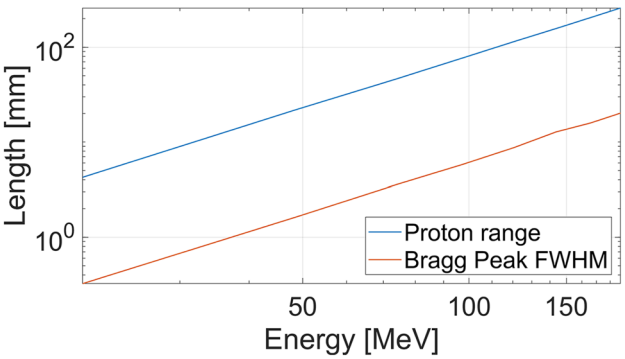

Fig. 3 Proton range and Bragg peak full-width at half maximum vs. proton beam energy. Increasing the beam energy and

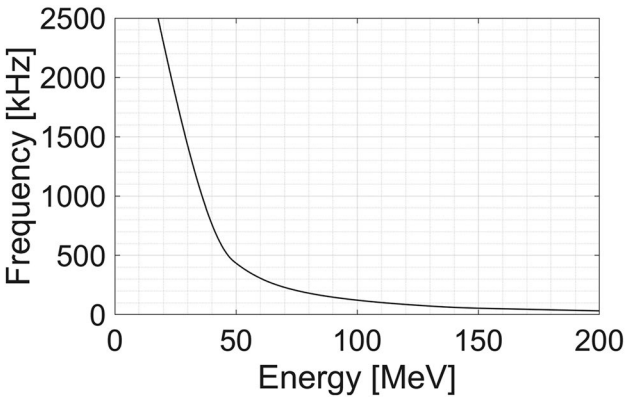

Fig. 4 Acoustic signal bandwidth dependency on proton beam energy

Table 1 Characteristics of a 60 meV clinical scenario

Parameter	Value
Proton energy	60 MeV
Protons per pulse	10^5
Beam range in water	38 mm
BP_{FWHM}	2.9 mm
Dose/pulse at BP	2 mGy/pulse
Pressure at BP	200 mPa
Pressure at AS	10 mPa
Signal frequency	330 kHz

propagation, resulting in a signal of a few tens of mPa at the surface of the acoustic sensor.

This paper focuses on a clinical scenario at 60 MeV and 2 mGy/pulse, characterized by an acoustic signal of 330 kHz of frequency and 200 mPa of pressure increase at the BP. The characteristics of the scenario and of the ionoacoustic signal are summarized in Table 1.

Proton Sound Detector Design

The sensor described here consists of a cylindrical water tank in acrylic glass (5 cm diameter, 5 mm wall thickness) surrounded by a circular array of 50 piezoelectric sensors glued to the acrylic by an epoxy resin. In Fig. 5, there are photos of the sensor. A 7 mm diameter hole was made in the acrylic glass into which a 100 µm thick Kapton entrance foil was fixed. This allows the beam to enter the water volume while minimizing the energy loss.

The internal sides of the piezoelectric crystals are connected to ground, while the external sides are individually wired (yellow wires) to be able to characterize each channel and to connect the detector to an analog front end to acquire the signals.

Frequency Response and Sensitivity

Ionoacoustic signals are typically sensed by piezoelectric sensors that transduce pressure variations into voltage variations. Piezoelectric sensors have a frequency response characterized by a passband and a resonance frequency, as shown in Fig. 6. The sensor has its maximum sensitivity at the resonant frequency, and it decreases by about 10 dB in the linear part of the frequency response. Lead–zirconate–titanate are among the most performing materials commercially available for such applications. This section refers to the PIC255 PZT produced by PiCeramics, whose characteristic parameters are listed in Table 2 [15]. The resonance frequency depends on the frequency coefficient N (1333 Hz·m) and on the thickness TH of the piezoelectric according to Eq. (1).

$$f_R = \frac{N}{Th}. \tag{1}$$

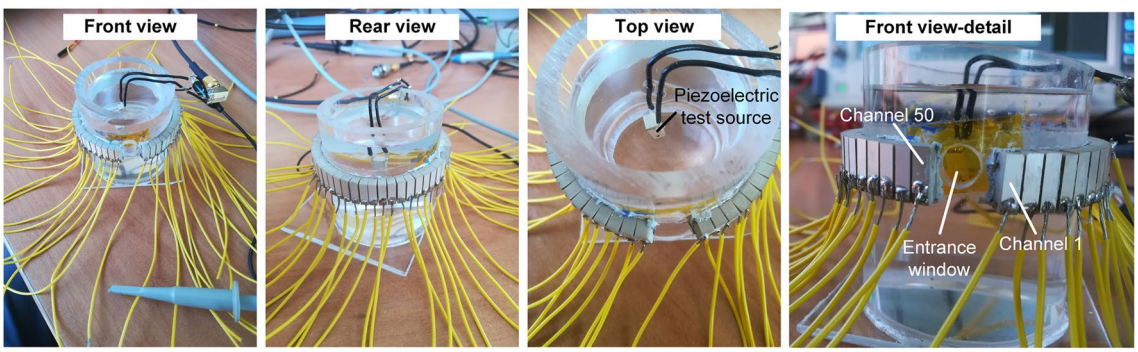

Fig. 5 Picture of a 60 MeV 50-channel ionoacoustic detector. A ring of 50 rectangular piezoelectric sensors is glued to an acrylic glass water container by means of an epoxy-metal powder glue (acoustic matching layer). All channels have the ground pins in common and a different Vout pin (yellow wires). The beam enters the tank through a Kapton entrance foil located in the sensors plane. A piezoelectric test source is placed inside the detector for characterization and acoustic testing

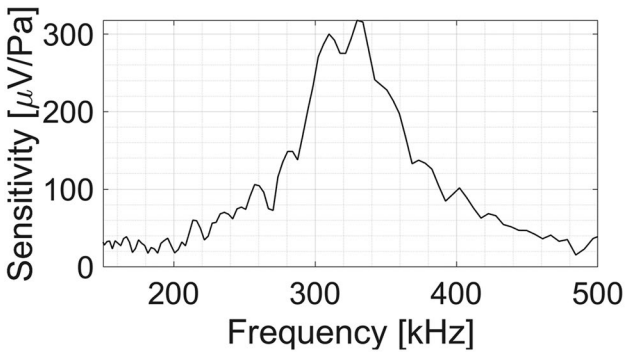

Fig. 6 Single-channel sensitivity (including matching layer)

A resonant frequency of 330 kHz was chosen in this case to match the signal frequency.

This sets the piezoelectric thickness to 4 mm and allows to calculate the in-band sensitivity using Eq. (2), where g_{33} is the piezoelectric voltage coefficient, equal to 25 mV/(Pa·m):

$$S_{PZT} = g_{33} \cdot TH. \tag{2}$$

Considering the 4 mm piezoelectric thickness, the PZT sensitivity is 100 µV/Pa. Considering the intrinsic gain at resonance, the piezoelectric sensitivity at 330 kHz increases by around 18 dB, thus improving the SNR but introducing ringing that, however, can be compensated for in post-processing. However, this sensitivity value is usually reduced to just 40% due to the acoustic impedance mismatch between the water (acoustic signal propagation medium) and the piezoelectric material itself. In fact, whenever an acoustic wave traveling in one medium encounters another medium with different mechanical properties, it is partly transmitted and partly reflected, as shown qualitatively in Fig. 7. The transmission coefficient η_T depends on the acoustic impedances of the materials (Z, defined as the product between density and speed of sound in the medium) and is equal to:

$$\eta_T = \sqrt{1 - \left(\frac{z_2 - z_1}{z_2 + z_1}\right)^2}. \tag{3}$$

Water has an acoustic impedance of 1.5 MRayl, very different from the 33 MRayl of the PZT, and therefore in a direct interface between the two materials only 40% of the wave amplitude is transmitted, causing a corresponding loss of sensitivity and SNR (−8 dB).

For this reason, an intermediate layer (called matching layer) is placed between the water and the piezoelectric to act as an impedance matching and increase the amplitude of the transmitted wave [18]. Using a single-layer matching material can increase the transmission coefficient to 57% if the matching material have an acoustic impedance equal to 7 MRayl.

However, suitable materials with 7 MRayl are difficult to obtain, and single-layer efficacy remains limited. For this reason, this detector exploits a 2-materials matching layer composed by the acrylic glass ($Z = 3.2$ MRayl) and an epoxy glue/metal powder mix ($Z = 8$ MRayl), achieving a 66% transmission coefficient and limiting the sensitivity loss to just 3.5 dB, improving the SNR by 4.5 dB w.r.t. direct water–PZT coupling.

The overall resonant sensitivity S (including piezoelectric sensitivity S_{PZT}, matching layer effects and resonant frequency gain G_r) is therefore equal to:

$$S = \eta_T \cdot g_{33} \cdot TH \cdot G_r. \tag{4}$$

This leads to a final AS sensitivity of 300 µV/Pa @ 330 kHz, as reported in Fig. 6.

Table 2 Piezoelectric characteristic parameters

Parameter	Symbol	Value
Frequency coefficient	Nf	1333 Hz·m
Resonant frequency	fr	330 kHz
Piezoelectric voltage coefficient	g_{33}	25 mV/(Pa·m)
Piezoelectric relative dielectric constant	ε_r	1750
Channel width	W	3 mm
Channel length	L	10 mm
Channel thickness	TH	4 mm
Water acoustic impedance	Z_w	1.5 MRayl
Acrylic glass acoustic impedance	Z_a	3.2 MRayl
Epoxy/metal powder glue acoustic impedance	Z_g	8 MRayl
PZT acoustic impedance	Z_{PZT}	34 MRayl
Sensitivity	S	300 µV/Pa

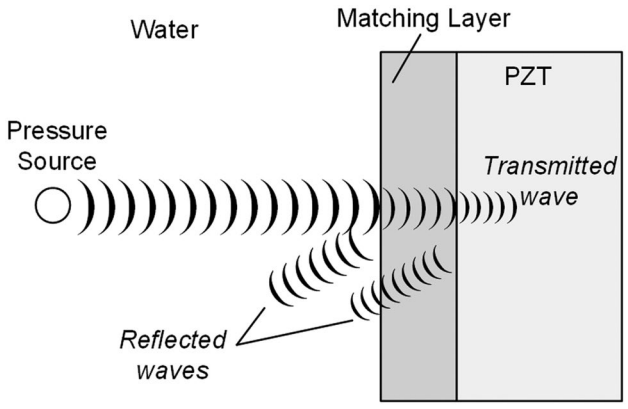

Fig. 7 Effect of acoustic impedance mismatch on wave transmission between different materials

Sensor Capacitance and Noise Power

Piezoelectrics are capacitive sensors and their output-referred noise power is equal to kT/C. For thin disk-shaped piezoelectrics, the capacitance can be estimated from the formula for a parallel-faced capacitor, where A is the piezoelectric area, ε_0 and ε_r are, respectively, the dielectric constants of the vacuum and relative dielectric constant of the piezoelectric material:

$$C = \varepsilon_0 \varepsilon_r \frac{A}{TH}. \tag{5}$$

Thus, the output-referred noise power of the sensor channel is:

$$ORN = \sqrt{\frac{kT}{C}} = \sqrt{\frac{kTTH}{\varepsilon_0 \varepsilon_r A}}. \tag{6}$$

Considering the physical parameters of the PZT, the single-channel capacitance is equal to 180 pF, leading to an output-referred noise power of 4.8 μV_{RMS}, which corresponds to 16 mPa_{RMS} input-referred noise power. The whole detector acts by combining (in digital domain) the signals from all channels, after re-phasing the signals time track to compensate for different time of arrivals (delay&sum). In this way, the independent random noise fluctuations from all channels are greatly reduced while the deterministic signal amplitude is preserved. This allows to decrease the noise power by $\sqrt{50}$, thus increasing the SNR by 17 dB and leading to a detector noise floor of 2.3 mPa_{RMS}.

$$IRN_{Nch} = \frac{ORN}{S} = \frac{1}{\eta_T \cdot g_{33} \cdot G_r} \sqrt{\frac{kT}{\varepsilon_0 \varepsilon_r ATHN_{ch}}}. \tag{7}$$

Such noise floor is enough to detect with 10 dB SNR a dose deposition at the detector center as low as 2 mGy.

Single-Channel Directivity

Ideal acoustic sensors are omnidirectional, i.e., they can acquire a signal regardless of its direction of arrival. However, real acoustic sensors are characterized by a certain amount of directivity, that is, they attenuate signals arriving from directions other than their axis. This characteristic, for a given frequency of the acoustic signal, depends on the difference between the size of the acoustic sensor (W, L) and the wavelength. In particular, if the acoustic sensor is small compared to the wavelength it behaves almost ideally (omnidirectional), while as its size increases it becomes more and more directive. Since the position of the Bragg peak is not known a priori, each channel cannot be previously oriented towards the BP. If the single channel is very directive, it significantly attenuates any off-axis signals, effectively lowering the AS sensitivity and final SNR.

This effect is represented in Fig. 8. The directivity of a single-channel element can be determined using the Fraunhofer laws of diffraction.

$$\frac{S(\theta)}{S} = dir(\theta) = sinc\left(\frac{\pi f L sin(\theta)}{c_w}\right). \tag{8}$$

Each channel has a rectangular shape with a small width to accept signals from all directions in the detector (horizontal) plane and a large length to reject signals from outside the detector plane and increase the SNR. The sensor width W is 3 mm, and its length L is 10 mm. The directivity patterns in the horizontal and vertical directions are represented in Fig. 9 in terms of sensitivity loss w.r.t. angle of arrival. Considering the 2.5 cm detector radius, the sensitivity loss is less than 3 dB for any source within a 1 cm diameter circle at the detector center.

Detector Validation and Experimental Results

Single-Channel Time of Flight Measurement

To validate the detector design presented in Section III and to show how a dedicated sensor can improve the Bragg peak localization performances, a sensor was designed for a specific experimental scenario present in literature, represented by a 60 MeV proton beam with 2 mGy dose deposition per beam pulse, in a scenario equivalent to what is found in literature and clinical practices. The physical environment was simulated using Geant4 to extract the 3D dose deposition profile and thus calculate the pressure increase spatial

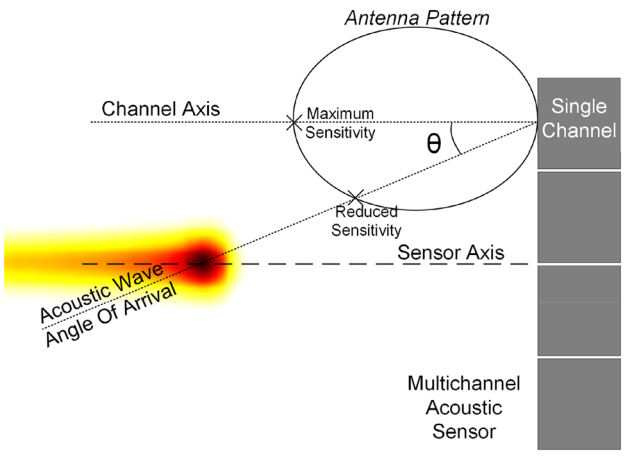

Fig. 8 Effect of misalignment between the acoustic source (Bragg peak) and the single-channel sensor axis

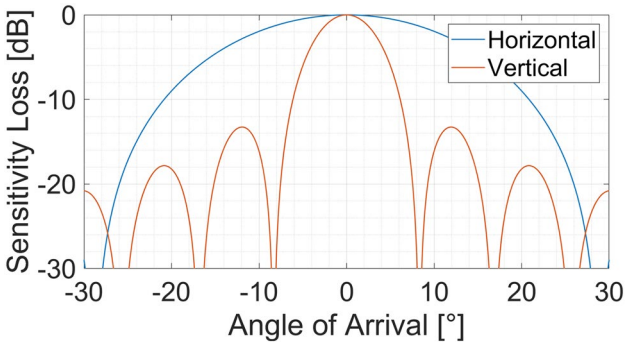

Fig. 9 Sensitivity loss vs. acoustic wave angle of arrival (antenna pattern) in horizontal and vertical direction w.r.t. the sensor axis (0°)

distribution [16]. k-Wave has then been used to simulate the pressure wave propagation in space and to determine the signal sensed by each channel of the sensor [17]. The output signals are shown in Fig. 10.

The pressure domain signals have been transformed into voltage domain by multiplying for the sensor sensitivity of 300 µV/Pa. Then the signal was band-passed to represent the sensor frequency response (330 kHz–3 dB frequency) and a band-limited thermal noise (sensor noise) was added. Figure 10-top shows the single-channel signal including sensor noise power, overlapped with the same signal without noise (dotted line). The very small dose deposition (2 mGy) leads to a negative SNR of − 7 dB and the signal is not recognizable from the noise background. Moreover, any band-pass filtering approach is not applicable because most of the noise power is within the signal bandwidth. The typical state of the art approach for such low-SNR scenarios is to average different beam pulses at the cost of a significant extra-dose not compatible with clinical treatments [2–5]. The result of the hereby proposed technique is shown in Fig. 10-bottom, where the space-domain average of the 50 signals (one per detector channel) is plotted against the noise-free signal (dotted line). The final SNR is 10 dB and the signal is clearly visible against the noise background. Such SNR value is enough to easily detect the acoustic wave peak to measure the time of flight and thus calculate the BP location with high precision. In particular, according to [8] a SNR value of 10 dB leads to a BP localization precision of 5.4% of the BP size (2.3 mm @ 60 MeV) which is 125 µm. This measurement precision is particularly relevant when compared to nuclear imaging techniques precision (several millimeters). Thanks to the spatial correlation enabled by multichannel sensors, such sub-millimeter precision can be achieved with a BP dose deposition as low as 2 mGy (a single beam pulse).

Multilateration for 2D Bragg Peak Localization

In addition to the increase in SNR, multichannel sensors can combine the temporal information of the individual channels to obtain a precise localization of the acoustic source (Bragg peak) in 2D. To this end, a multilateration algorithm was applied to the 50 signals coming from the sensor channels. Multilateration calculates the position of the sound source starting from the difference in the arrival time of the signal (proportional to the distance between the source and the channel) to each channel. To validate the detector's behavior, a piezoelectric test source was placed inside the detector's water volume and used as a transmitter, stimulating it with a single sinusoid period (at 330 kHz) of 1 $V_{0\text{-peak}}$ amplitude. The piezoelectric test source has the same physical characteristics as each sensor channel and was waterproofed with a thin polish coating. The signals acquired by each channel are shown in Fig. 11. A different offset was applied to each channel for ease of representation. The channels are sorted from 1 (top) to 50 (bottom), where channel 1 is the first channel to the right of the entry window and the other channels are in counterclockwise order. Each channel signal has a slightly different phase because the distance between the acoustic source (BP) and the channels are different, and

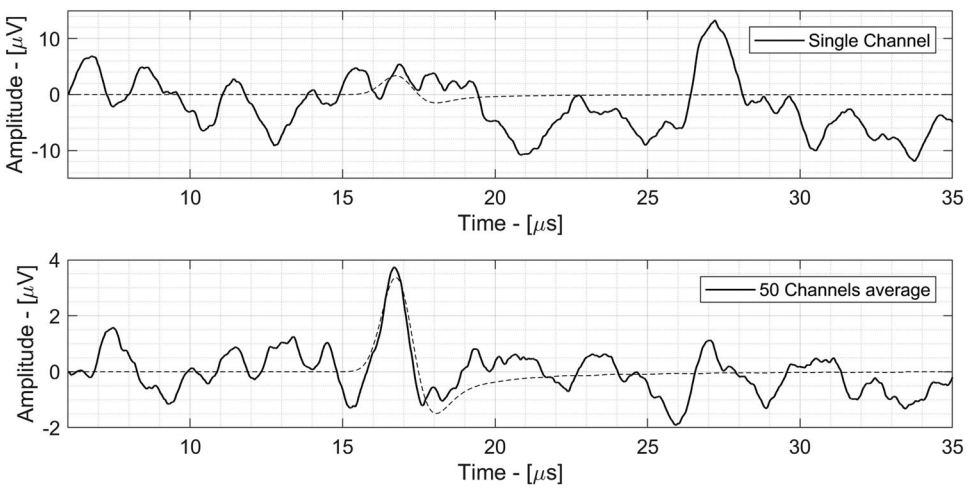

Fig. 10 Cross-domain (Geant4/k-Wave/Matlab) simulation of the multichannel detector. TOP: single-channel output with sensor noise power with − 7 dB SNR. BOTTOM: 50-channels spatial average (detector output) with + 10 dB final SNR

consequently the ToF. The signal exhibits some ringing due to the undamped piezoelectric source. Moreover, the signal maximum amplitude oscillates between a maximum value, while some channels exhibit a very small amplitude. This difference in amplitude is caused by the shape of the sound source. In fact, since the piezoelectric has a square section, its directivity leads it to transmit the acoustic signal mainly in the directions perpendicular to its faces, while little acoustic power is sent in a diagonal direction (Table 3).

Furthermore, the mechanical contraction of the piezoelectric generates an acoustic signal that starts with a positive peak in the directions parallel to the polarization of the crystal (front and rear face of the piezoelectric), while the acoustic signal generated in the directions perpendicular to the polarization of the piezoelectric begins with a peak of negative pressure. These non-idealities of the acoustic signal are not present in the ionoacoustic signal generated by a particle beam, but represent an acceptable trade-off in the face of the simplicity of the testbench, to validate the detector in the laboratory before carrying out tests with proton beams at particle accelerator facilities. Despite the non-ideality of the signal, the multichannel characteristic of the detector makes it sufficiently robust to locate the acoustic source with high accuracy. Figure 12 shows the result of the multilateration algorithm [19], where the position of each channel is shown with a blue asterisk (detector seen from above, entrance window on the left side) and the center of the detector is marked with a red circle. The position calculated by the algorithm is shown with a black X, located at ($x_{BP} = +2.6$ mm; $y_{BP} = +2.2$ mm), where (0; 0) is the detector center. The position was compared with the position of the physical source (measured with a caliper) and is compatible within experimental errors (< 1 mm).

Table 3 Summary of experimental results

Parameter	Value
Single-channel SNR	− 7 dB
50-channels SNR	10 dB
BP Localization precision	125 µm
Relative precision (w.r.t. proton range)	3%
Dose for x precision	2 mGy
Measured source X position	+2.6 mm
Measured source Y position	+2.2 mm
Accuracy	< 1 mm

Discussion and Conclusions

This paper presents the design and the experimental validation of a multichannel detector for the characterization of proton beams through the ionacoustic effect. The detector was optimized for 60 MeV proton beams (corresponding to the lowest range of energies used in the clinical setting) and validated with cross-domain simulations and with an acoustic testbench, in preparation for a subsequent test at a particle accelerator facility. The design strategy of this detector is based on using a multichannel approach to reduce the noise power without requiring an extra dose, as opposed to what is done in state of the art where single-channel sensors require averaging of several beam pulses to improve the SNR, involving an extra dose that does not allow to apply this technique in clinical contexts. This low SNR is what currently limits the application of this technique as a tool for calibration and real-time control of the beams in hadron therapy treatments. This paper aims to show how

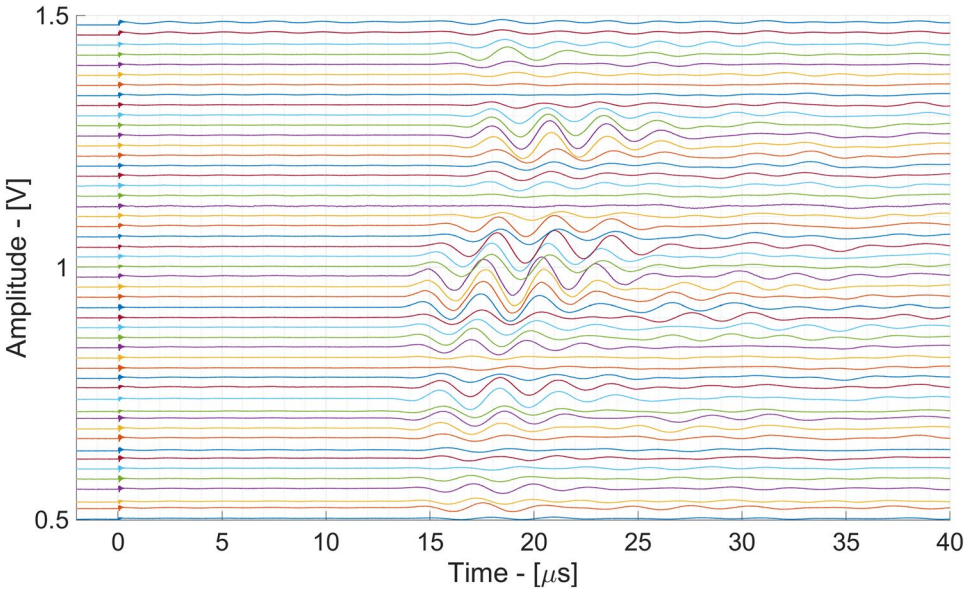

Fig. 11 Output signals from each detector channel (channels 1–50 from top to bottom) with piezoelectric test source

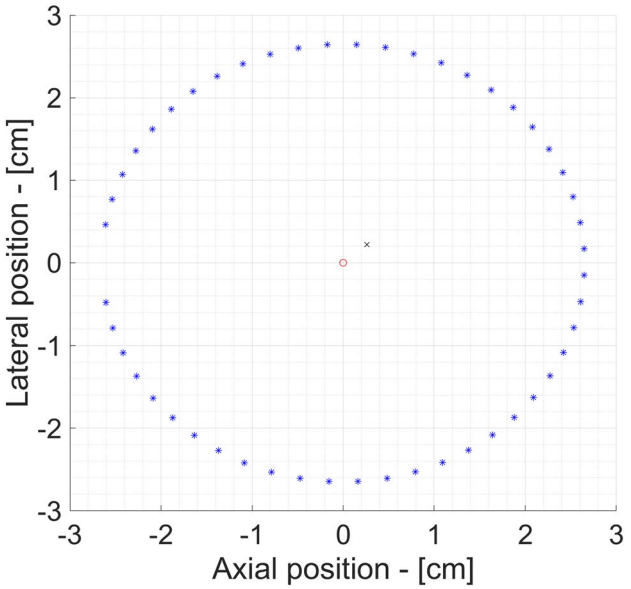

Fig. 12 Multilateration algorithm output with sensors positions (blue asterisks), detector center (red circle) and test source location (black cross)

a new generation of dedicated ionacoustic detectors can overcome this obstacle through the use of dedicated multichannel detectors that achieve very low noise powers, not possible with a single-channel approach. However, the use of multichannel sensors requires parallel hardware-based signal acquisition and processing (analog and digital). For this reason, the development of dedicated integrated circuits is essential to reduce size, power consumption, crosstalk between channels and in general acquire in parallel the signals while preserving the SNR. Finally, multilateration or acoustic imaging algorithms are needed to combine signals from multiple channels and obtain spatial 2/3D information on the energy deposition of the beam.

Funding Open access funding provided by Università degli Studi di Milano - Bicocca within the CRUI-CARE Agreement. This work was partially supported by the Proton Sound Detector and Ionotrack projects founded by the Italian Institute for Nuclear Physics (INFN).

Declarations

Conflict of Interest On behalf of all authors, the corresponding author states that there is no conflict of interest.

References

1. Knoll GF. Radiation detection and measurement. Wiley; 2010.
2. Sulak L, et al. Experimental studies of the acoustic signature of proton beams traversing fluid media. Nucl Inst Methods. 1979;161(2):203–17.
3. Hayakawa Y, et al. Acoustic pulse generated in a patient during treatment by pulsed proton radiation beam. Radiat Oncol Investig. 1995;3:42–5.
4. Assmann W, et al. Ionoacoustic characterization of the proton Bragg peak with submillimeter accuracy. Med Phys. 2015;42(2):567–74.
5. Stephan K, et al. Ionoacoustic tomography of the proton Bragg peak in combination with ultrasound and optoacoustic imaging. Sci Rep. 2016;6(1):1–7.
6. Knopf A, et al. In vivo proton range verification: a review. Phys Med Biol. 2013;58:R131.
7. Vallicelli EA, et al. 22 dB signal-to-noise ratio real-time proton sound detector for experimental beam range verification. IEEE Trans Circ Sys I: Regul Papers. 2020;68(1):3–13.
8. Vallicelli EA, De Matteis M. Analog filters design for improving precision in proton sound detectors. J Low Power Electron Appl. 2021;11(1):12.
9. E. Vallicelli, et al., 2021 "Front-end Design Optimization for Ionoacoustic 200 MeV Protons Beam Monitoring", In Proc. of the 14th Intern. Joint Conf. on Bio. Eng. Syst. and Tech., vol. 1, pp. 77–87.
10. Julie L, et al. Investigating the accuracy of co-registered ionoacoustic and ultrasound images in pulsed proton beams. Phys Med Biol. 2021;66(18):185007.
11. Vallicelli EA, et al. A 0.3 nV/$\sqrt{}$ Hz input-referred-noise analog front-end for radiation-induced thermo-acoustic pulses. Integration. 2020;74:11–8.
12. Michele R, et al. Acoustic analog front end for proton range detection in hadron therapy. IEEE trans Biomed Circ Sys. 2018;12(4):954–62.
13. de Marcello M, et al. Proton induced thermoacoustic process as linear time invariant system. IEEE Trans Radiat Plasma Med Sci. 2021;6:336–44.
14. de Marcello M, Baschirotto A, Vallicelli E. Acoustic analog signal processing for 20 MeV-200 MeV proton sound detectors. IEEE Trans Radiat Plasma Med Sci. 2021;6:325–35.
15. PI Ceramic GmbH. https://www.piceramic.com/en/products/piezoceramic-components/disks-rods-and-cylinders/piezoelectric-discs-1206710#specification. Accessed 12 Jan 2024.
16. Agostinelli S, et al. "GEANT4-a simulation toolkit." Nuclear Instr and Meth Physics Res Sec A. 2003;506:250–303.

17. Treeby BE, Cox BT. k-Wave: MATLAB toolbox for the simulation and reconstruction of photoacoustic wave fields. J Biomed Opt. 2010;15(2): 021314.
18. Rathod VT. A review of acoustic impedance matching techniques for piezoelectric sensors and transducers. Sensors. 2020;20(14):4051.
19. William M, Hereman W. Determination of a position in three dimensions using trilateration and approximate distances. Dep Math Comput Sci, Colorado School of Mines, Golden, Colorado, MCS-95. 1995;7:19.